Elastic 3D full-waveform inversion

Lluís Guasch, Mike Warner*, Tenice Nangoo, Jo Morgan, Adrian Umpleby, Ivan Stekl, Nikhil Shah
(Imperial College London)

Summary

We demonstrate the application of elastic 3D full-waveform inversion (FWI) to a field dataset. We first analyze and validate its performance using synthetic data generated from a 3D version of the Marmousi model. We show that elastic FWI can recover both p-wave and shear-wave velocity models using only single-component hydrophone data. We then apply elastic FWI to a 3D multi-component OBC air-gun dataset from the North Sea, and show that it successfully recovers both the p-wave and shear-wave velocity structure of shallow channels.

Introduction

Full-waveform inversion of 3D seismic data is becoming increasingly prominent, both as a means of building high-resolution velocity models for depth migration, and for the generation of accurate models of physical properties that can be interpreted directly. Invariably, when 3D FWI is applied to field data, the acoustic approximation to the wave equation is employed, whereas the real world can be more accurately described by a fully elastic wave equation.

Warner *et al* (2012) show that the acoustic wave equation is sufficient for FWI provided that the purpose is to generate p-wave velocity models for depth migration, and provided that the inversion is limited principally to early refracted arrivals and to the phase rather than the absolute amplitudes of the field data. However, to extract fully quantitative models that go beyond p-wave velocity, to use amplitudes properly, or to use later mid-offset arrivals, requires the use of more-complete physics in the forward modeling. The elastic wave equation is an important part of this, but attenuation, anisotropy and a proper account of density variation can also be important. Here we deal only with elastic effects.

We have developed a 3D forward modeling code that solves the isotropic heterogeneous elastic wave equation by using fourth-order finite differences, time-stepping on a staggered grid. We can simulate a variety of single and multi-component sources and receivers, and can include both a free surface and perfectly matched boundary layers. We use this code to form the kernel of a full-waveform inversion scheme in which we can invert, either simultaneously or separately, for a variety of parameters. In this study, we invert for p-wave and shear-wave velocity independently, and keep a fixed relationship between density and p-wave velocity. The code is parallelized.

Application to a 3D synthetic model

The 2D Marmousi model has been used widely to test FWI, and there is much experience with models of this kind. We therefore build a fully three-dimensional and elastic version of Marmousi, Figure 1, to test and validate our elastic inversion codes. The 3D model was built by initially extending the 2D p-wave Marmousi model in the third dimension, then shearing this volume successively in three directions with a spatially variable degree of shear. Successive in-lines look superficially like the original model, but they differ in detail, they vary in the cross-line direction, there are moderate cross-dips, and strike and dip directions vary fully in 3D.

The shear-wave model has the same structure as the p-wave model, but the Vp/Vs ratio varies around the model, and is a combined function of Vp and of depth. Vp/Vs values vary spatially from about 1.7 to 2.0. The model has a shallow water layer at the top which has no shear strength, and all sources and receivers were located within the water layer below a free reflecting upper surface. There is a fixed relationship between p-wave velocity and density, and there is no attenuation or anisotropy in the model.

Figure 2 shows an acoustic and a fully elastic 3D shot record generated using this model. It is immediately apparent from this figure that the elastic record is more complicated than the acoustic record. Although the source is a pure explosion, and the receivers are purely hydro-phones, doubly converted p-wave and other elastic effects add a significant coda to the acoustic records, and change their AVO and other amplitude characteristics. They do not however affect the arrival times of the main p-wave phases which is why acoustic FWI is effective when it is parameterized appropriately.
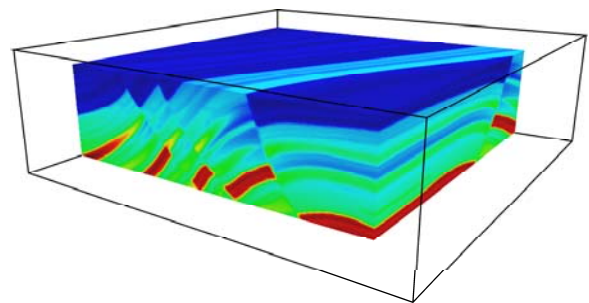
Figure 1 A cut-away view of part of the 3D Marmousi model.

Elastic 3D FWI
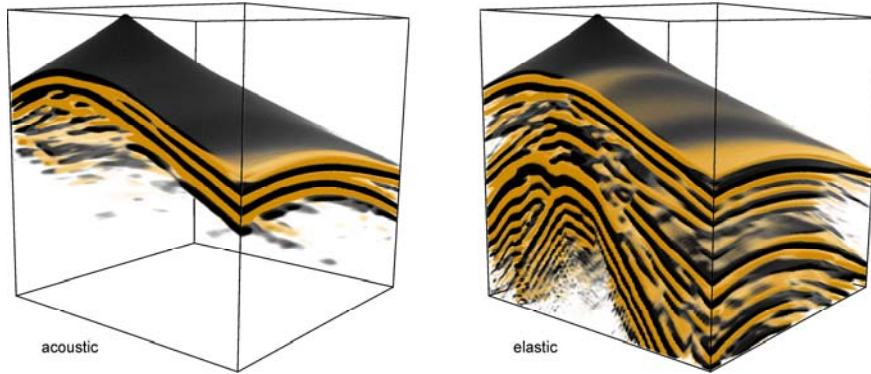
Figure 2 A gather generated by a single source in acoustic and elastic versions of the 3D Marmousi model. The source and the receivers are located within the water layer; the late elastic arrivals are mostly doubly converted p-waves since no shear-waves are recorded directly.

We generated time-domain synthetic data within this model, for 240 p-wave sources recorded on about 10,000 hydrophone receivers regularly distributed within the water layer. The geometry approximates that of a 3D OBH dataset after the application of source-receiver reciprocity. We inverted these data successively at seven frequencies from 3 to 9 Hz. We applied trace equalization to all data during the inversion to simulate better our practice with field data. We ran a total of 35 iterations, inverting independently and simultaneously for both p-wave and shear-wave velocities. We preconditioned the gradient using an approximate diagonal Hessian.

Figure 3 shows the results obtained by elastically inverting the elastic data to obtain p-wave velocity. The resolution and continuity of the recovered models is similar to that obtained by acoustic inversion of acoustic data; it is limited principally by the finite bandwidth, finite aperture, and source spacing of the original seismic data.

Figure 4 shows the recovery of shear-wave velocity; the panels are the same as those shown in Figure 3. These inversions are obtained using only p-wave sources and hydrophone receivers. However the data do contain strong doubly converted p-s-p waves, converted both at the sharp

1500   Vp (m/s)   3750
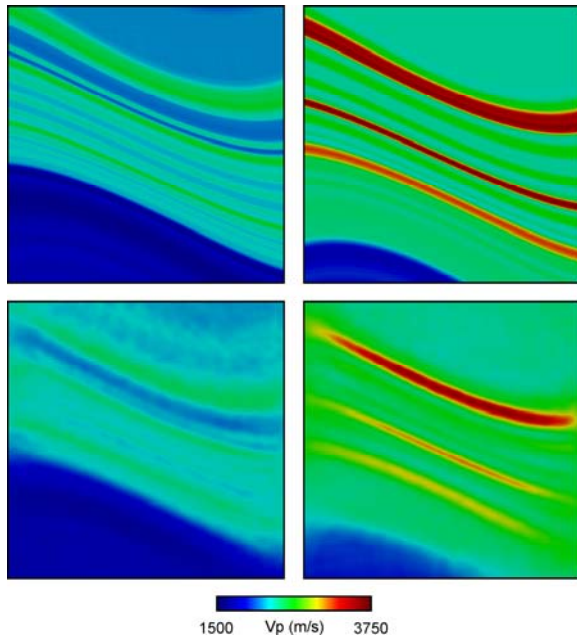
Figure 3 Horizontal depth slices showing the recovery of p-wave velocity. Upper panels show the true model; lower panels show the recovered model. Left panels at 720 m depth; right panels at 1000 m depth. Model measures 4800 × 4800 m.

770   Vs (m/s)   2212
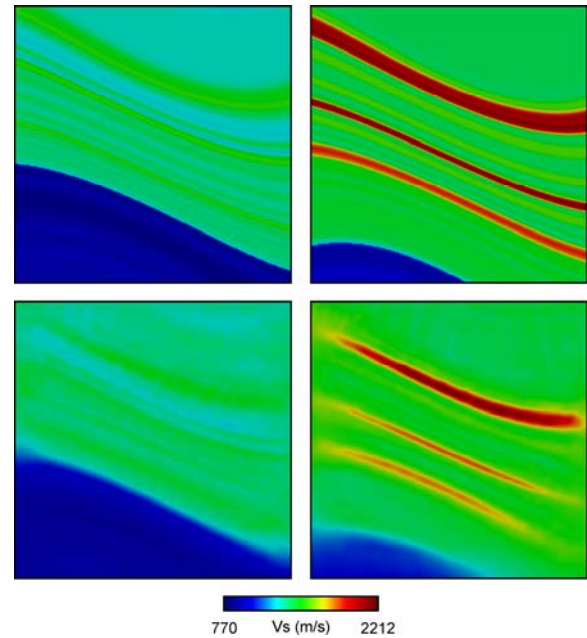
Figure 4 Horizontal depth slices showing the recovery of shear-wave velocity. Upper panels show the true model; lower panels show the recovered model. Left panels at 720 m depth; right panels at 1000 m depth. Model measures 4800 × 4800 m.

sea bottom and from structure deeper within the model. Although the shear-wave structure does influence the amplitudes and waveforms of the pure p-waves, it is principally these doubly converted waves that provide the shear-wave imaging.

In principle, the shear images should be sharper than the p-wave results because the seismic wavelength is shorted for the shear-waves. In this experiment, we do not appear to see that effect, and the two images are similar in their resolution. One difference that is clear however is the somewhat higher noise level in the p-wave images. This surprising result appears to be related to the original source spacing which influences the p-wave recovery more strongly than it does the recovered shear-wave model.

It is well known that imaging using multiple scattering (typically free-surface multiples) can compensate for sparsity in field data (e.g. Berkhout & Verschuur, 2006). We speculate that we are seeing an analogous effect related to p-s conversions; in the p-wave images, the primary p-waves dominate the results, and these are sparse, whereas in the shear-wave results, many low-amplitude conversions contribute to the quality of the final image.

Figure 5 shows a more familiar vertical section through the 3D Marmousi model in the dip (in-line) direction. These images are for shear-wave velocity. The images are significantly less well resolved than are the p-wave images. This is especially true in the upper portions of the model where fine layering, which is commonly recovered by
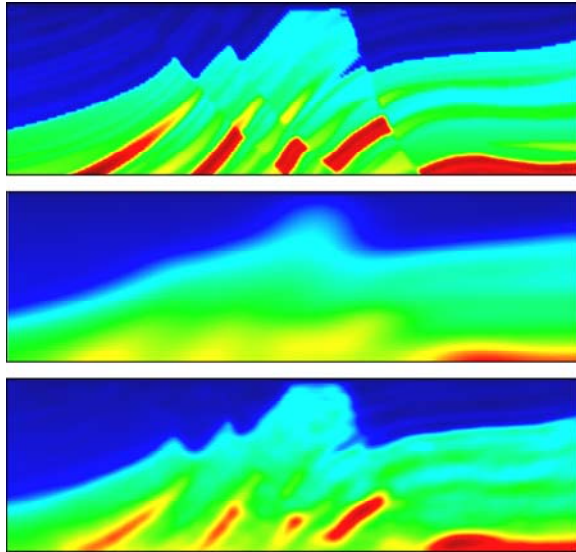
acoustic or elastic p-wave imaging, is not recovered in these shear images. However, given that there are no shear sources or shear-wave receivers in this dataset, the recovery of shear-velocity is remarkably good.

In Figure 5, it is not just the structure that is recovered, but also the absolute shear-velocities. This is important because the p and s models have the same structure. The Vp/Vs ratio though varies around the model, and cross-talk of the p-wave model into the shear-wave model would not be able to explain the absolute shear velocities correctly.

Figure 6 shows shear-wave sections in the nominal strike (cross-line) direction. These plots provide a good indication of the degree of three-dimensionality in the synthetic model – there is evidently significant cross-line structure. In the synthetic experiment, the source array was confined to approximately the central half of the model in the cross-line direction. The effects of this are evident in the recovered model; the resolution decays away from the central region as the fold, offset and azimuthal coverage all shrink at the edges of the model.

Although it is not immediately clear from the images in Figures 5 & 6, elastic inversion can be significantly compromised by surface and interface waves. In these data, at the lowest frequencies, strong Scholte waves are generated at the sea bed, and these are problematic during the inversion. In principle, they can be inverted, but in practice they are strongly non-linear and confuse the FWI.
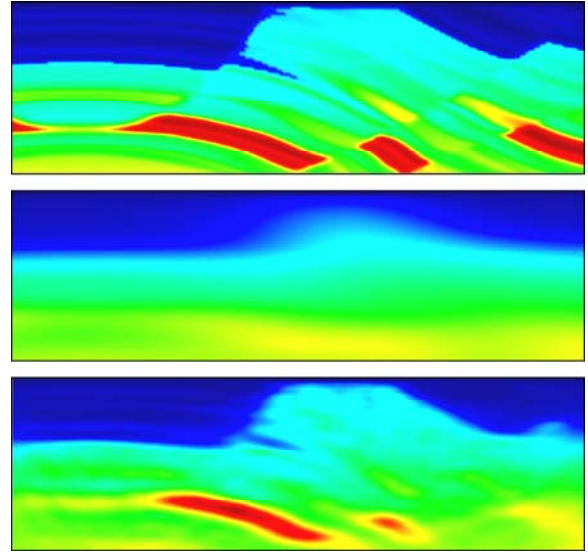

Figure 5 A vertical slice in the nominal dip (in-line) direction down the center of the shear-wave model. Upper panel shows the true model; center panel shows the starting model; lower panel shows the recovered model. Velocity scale as in Figure 4.

Figure 6 A vertical slice in the nominal strike (cross-line) direction through the shear-wave model. Upper panel shows the true model; center panel shows the starting model; lower panel shows the recovered model. Velocity scale as in Figure 4.

Full 3D field data example

Having demonstrated that full elastic inversion is viable in 3D on idealized synthetic data, we have applied elastic FWI to a full 3D field dataset. The dataset that we used to do this is from a four-component OBC survey, acquired using airguns in the North Sea (Nangoo *et al*, 2012).

In common with many other datasets, these data are affected by anisotropy. We have previously inverted them using anisotropic acoustic FWI, and it is clear that proper account of anisotropy is required in order to invert these data accurately. The data are also undoubtedly affected by attenuation which has a strong influence upon absolute amplitudes and upon the decay of amplitude with time.

Warner *et al* (2012) show that both anisotropy and attenuation should properly be taken into account during FWI in order to produce fully quantitative models. Our 3D elastic code is isotropic and it does not allow for attenuation, and so we are unable to account for these effects accurately. We normalized amplitudes and matched the source spectrum to the field data, and this mitigates the effects of attenuation somewhat. We also concentrate here on imaging only shallow structure where anisotropy is largely absent.
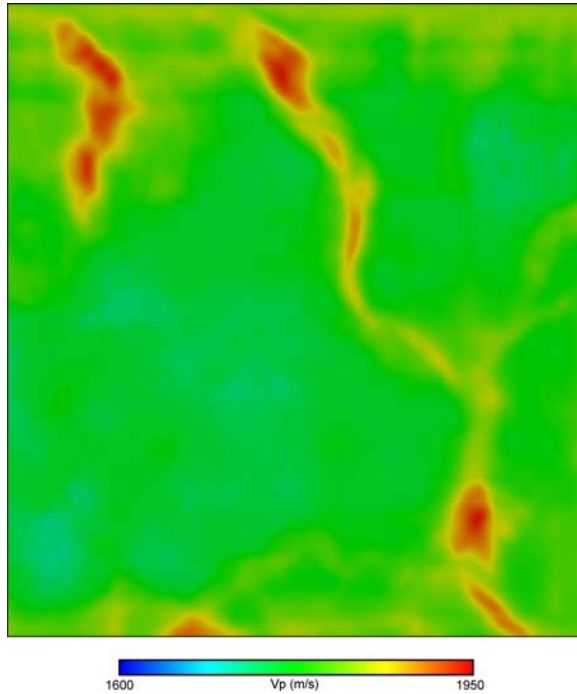
Figure 7 A horizontal depth slice through the recovered p-wave velocity model showing shallow buried glacial channels. The section is 250 m below the seabed, and is about 10×12 km.
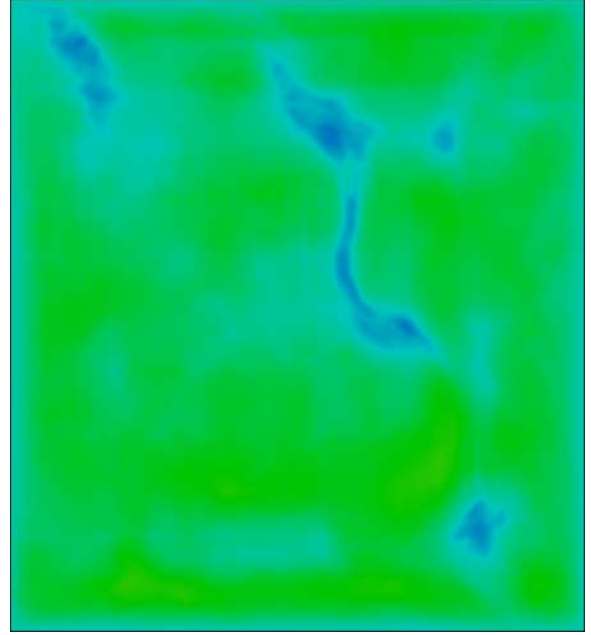
Figure 8 A horizontal depth slice through the recovered s-wave velocity model corresponding to the p-wave image in Figure 7.

Figure 7 and Figure 8 show p-wave and shear-wave images respectively of shallow channels buried in the top few hundred meters of the subsurface; we also see these in the reflection data. Interestingly the channels appear as high-velocity features for p-waves, but as low-velocity features for s-waves. This means that there is a significant change in Vp/Vs within the channels. It also implies that reflection imaging using converted waves may be compromised beneath such features if the shear-velocities used to process and migrate the data are derived from p-wave velocities.

The p and s channels do not exactly coincide. We do not yet know if this mismatch is real, indicating perhaps complex channel morphologies and infill, or if our shear-wave imaging is less than perfect. The lack of coincidence however gives us some confidence that we are not simply imaging cross talk that maps a p-wave velocity anomaly spuriously into a shear-wave anomaly. We are continuing to work on these data to refine and validate the images.

Conclusions

We have a methodology and a parallel computer code than can successfully undertake full-elastic 3D full-waveform inversion on realistic single and multi-component datasets. We have proved its performance on synthetic data, and we have applied it to a full 3D multi-component OBC dataset, obtaining plausible images of in-filled glacial channels. So far as we are aware, this is the first application of elastic 3D full-waveform inversion to a full-scale field dataset.